Research Article

Lv Feng, Ziyi Su, Ruohu Zhang, Zhigang Li, Bingjue Li and Guanghao Rui*

Anomalous optical gradient force induced by polarization-tuned antisymmetry in energy density gradient

https://doi.org/10.1515/nanoph-2025-0223
Received May 15, 2025; accepted August 10, 2025;
published online September 10, 2025

Abstract: The spatial inhomogeneity of electromagnetic energy density in an optical field typically gives rise to conservative gradient forces, which serve as the fundamental mechanism for trapping nanoparticles in optical tweezers. Surprisingly, however, we demonstrate that even in the absence of an energy density gradient, optical gradient forces can still act on isotropic, achiral particles when the incident field consists of counter-propagating plane waves engineered to exhibit polarization-controlled antisymmetry between the electric and magnetic energy density gradients. Through both numerical simulations and analytical derivations based on multipole expansion theory, we show that this anomalous gradient force arises from the electromagnetic symmetry breaking induced by the particle itself, irrespective of its size. Notably, this electromagnetic symmetry breaking-induced gradient force reaches its maximum under elliptical polarization at the specific position, rather than linear or circular polarization, underscoring the critical role of polarization configuration in modulating energy density gradients. These findings reveal a previously unrecognized mechanism for optical gradient force generation and deepen our understanding of the role of hidden antisymmetry in structured light fields.

Keywords: optical tweezers; optical gradient force; energy density gradient; polarization; electromagnetic symmetry

1 Introduction

The momentum transfer effect in light–matter interactions constitutes a fundamental physical phenomenon in the research of optical force [1]–[3]. Over the past decade, significant advancements in optical field manipulation technologies have propelled the study of micro- and nanoparticle dynamics to new heights [4]–[7]. Among the various manifestations of optical forces, radiation pressure emerges as the most intuitive mechanical effect, its theoretical origins tracing back to Kepler's astronomical explanation of the directional behavior of comet tails [8]. A landmark breakthrough was achieved in 1970, when Ashkin successfully demonstrated laser trapping and manipulation of micron-sized particles through the use of two opposing beams [9]. Building on this, Ashkin further developed three-dimensional optical trapping technology using a single, tightly focused laser beam [10]. This pioneering work not only laid the physical foundation for optical tweezers but also unveiled optical gradient force as a novel and profound mechanism governing light–matter interactions.

With the rapid development of micro- and nanophotonics, the application scope of optical gradient forces has expanded beyond fundamental physics research into diverse fields [11]–[18] such as biomedicine and materials science, enabling the precise manipulation of particles across a broad size range, from the nanoscale to the microscale, encompassing birefringent crystals [16], biological cells [17], and chiral molecules [18]. Particularly noteworthy is the emergence of long-range optical pulling forces arising from negative optical field gradients [19], as well as enantioselective trapping techniques within chiral gradient force fields [20]–[24], both of which underscore the unique advantages of spatially modulated optical fields in the manipulation of complex particles. Theoretical investigations have further revealed that the generation of

Lv Feng and Ziyi Su contributed equally to the paper.

***Corresponding author: Guanghao Rui**, Department of Optical Engineering, School of Electronic Science and Engineering, Southeast University, Nanjing, Jiangsu, 211189, China; E-mail: ghrui@seu.edu.cn
Lv Feng, **Ziyi Su**, **Ruohu Zhang and Zhigang Li**, Department of Optical Engineering, School of Electronic Science and Engineering, Southeast University, Nanjing, Jiangsu, 211189, China,
E-mail: lvfengphy@163.com (L. Feng), ziyisu_seu@163.com (Z. Su), zrh@seu.edu.cn (R. Zhang), zhigang5456@seu.edu.cn (Z. Li).
https://orcid.org/0000-0002-3895-6468 (L. Feng)
Bingjue Li, School of Mechanical Engineering, Southeast University, Nanjing, Jiangsu, 211189, China, E-mail: libj@seu.edu.cn

chiral gradient forces is intrinsically linked to the gradient of magnetoelectric energy density [25]. In the case of achiral Rayleigh particles, the underlying force mechanism extends beyond the conventional intensity gradient (the electromagnetic energy density gradient) to incorporate the synergistic influence of the phase gradient [26]–[28]. Under the paraxial approximation, particular significance is the observation that the electromagnetic energy density gradient reflects the dual symmetry properties of the underlying electric and magnetic fields [29], [30]. However, early theoretical models attributed the gradient force on nonmagnetic particles solely to the electric field energy gradient [31]–[33], thereby confining the interpretation of local dynamic characteristics to electrical components. This restriction is now understood to stem from the dual asymmetry inherent in local light–matter interactions.

In this work, we demonstrate that an isotropic, achiral spherical particle can experience a counter-intuitive longitudinal gradient force, even when the illuminating field exhibits no net energy density gradient. This phenomenon is enabled by the polarization-tuned antisymmetry between the electric and magnetic components of the energy density gradient of the light field. Unlike conventional gradient forces that arise directly from spatial intensity variations, the force observed here originates from the symmetry breaking of the electromagnetic induced by the presence of the particle. This mechanism is revealed through a comprehensive analysis valid for the particle of arbitrary size. Remarkably, by tuning the incident angle and adjusting the polarization orientation of the incoming light, the antisymmetric distribution of electric and magnetic energy density gradients can be disrupted, generating a gradient force acting on the particle with the electromagnetic symmetry. Furthermore, the electromagnetic symmetry-breaking induced gradient force reaches its maximum under elliptical polarization at the specific position, rather than under linearly or circularly polarized light. By precisely modulating the particle radius, we isolate the respective contributions of electric and magnetic energy density gradients to the overall force, offering deeper insight into the fundamental mechanisms at play. These findings not only advance our understanding of polarization-mediated optical gradient forces but also open new avenues for applications in optical field characterization and light-driven particle manipulation.

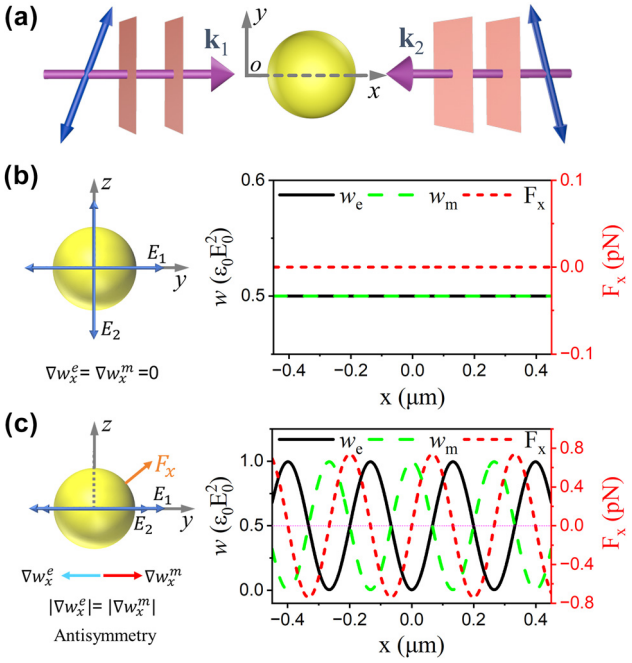

Figure 1: Schematic illustration of the longitudinal optical force arising from polarization-tuned antisymmetry in a two-wave interference field. (a) An achiral spherical particle is illuminated by a standing wave formed by two counter-propagating plane waves with linear polarizations. (b, c) The longitudinal optical force and the corresponding electric and magnetic energy densities as functions of the particle position, for incident fields with (b) orthogonal (y- and z-) polarizations and (c) identical (y-) polarizations. The incident wavelength is 532 nm. The particle has a radius of 400 nm and is immersed in vacuum, with a relative permittivity of 2.53 and relative permeability of 1.0.

2 Results and discussion

To illustrate the anomalous gradient force, an isotropic particle is considered to be immersed in an interference field generated by two counter-propagating plane waves with identical amplitude $E_0 = 8.6832 \times 10^5$ V/m, wavelength $\lambda = 532$ nm, and wave vectors oriented along the x-axis (as shown in Figure 1a). The resulting electric field of the interference pattern is expressed as $\mathbf{E} = E_0\boldsymbol{\mathcal{E}}_1 e^{i\mathbf{k}_1\cdot\mathbf{r}} + E_0\boldsymbol{\mathcal{E}}_2 e^{i\mathbf{k}_2\cdot\mathbf{r}}$, where $\mathbf{k}_j = kcos(\varphi_j)\hat{\boldsymbol{x}}$ denotes the wave vector of the j-th plane wave, k is the wave number in vacuum, and position vector is given by $\mathbf{r} = x\hat{\boldsymbol{x}} + y\hat{\boldsymbol{y}} + z\hat{\boldsymbol{z}}$. The complex amplitude of each plane wave is described by $\boldsymbol{\mathcal{E}}_j = \sin(\alpha_j)e^{i\beta_j}\cos(\varphi_j)\hat{\boldsymbol{y}} - \cos(\alpha_j)\hat{\boldsymbol{z}}$ where φ_j is the angle between the wave vector and the x-axis, viz. $\varphi_{1,2} = 0, \pi$, α_j describes the angle between the electric field direction and the z-axis, and β_j indicates the phase difference between the z and y components of the electric field. The energy density of optical field is expressed as [34]:

$$w = \frac{1}{4}\left(\varepsilon_0|\mathbf{E}|^2 + \mu_0|\mathbf{H}|^2\right) = w_e + w_m, \tag{1}$$

where ε_0 and μ_0 are the permittivity and permeability in the vacuum, respectively, and w_e and w_m are the electric and magnetic parts of the energy density, given by:

$$
\begin{aligned}
w_e &= \frac{\varepsilon_0 E_0^2}{2}\big[1+\cos\alpha_1\cos\alpha_2\cos(2kx)\\
&\quad -\sin\alpha_1\sin\alpha_2\cos(2kx+\beta_1-\beta_2)\big],\\
w_m &= \frac{\varepsilon_0 E_0^2}{2}\big[1-\cos\alpha_1\cos\alpha_2\cos(2kx)\\
&\quad +\sin\alpha_1\sin\alpha_2\cos(2kx+\beta_1-\beta_2)\big].
\end{aligned}
\tag{2}
$$

Accordingly, the x-component of the electric and magnetic energy density gradients (∇w_x^e and ∇w_x^m) are expressed as:

$$
\begin{aligned}
\nabla w_x^e &= E_0^2 k\varepsilon_0\big[-\cos\alpha_1\cos\alpha_2\sin(2kx)\\
&\quad +\sin\alpha_1\sin\alpha_2\sin(2kx+\beta_1-\beta_2)\big],\\
\nabla w_x^m &= E_0^2 k\,\varepsilon_0\big[\cos\alpha_1\cos\alpha_2\sin(2kx)\\
&\quad -\sin\alpha_1\sin\alpha_2\sin(2kx+\beta_1-\beta_2)\big].
\end{aligned}
\tag{3}
$$

It can be clearly observed that the total energy density remains constant ($w=\varepsilon_0 E_0^2$) for illumination with arbitrary polarization states, resulting in a vanishing total energy density gradient, i.e., $\nabla w_x = \nabla w_x^e + \nabla w_x^m = 0$. This condition can be classified into two cases. First, when the polarization directions of the two plane waves are orthogonal (i.e., $\alpha_1=\pi/2$ and $\alpha_2=0$), both the electric and magnetic energy densities remain spatially uniform ($w_e=w_m=\varepsilon_0 E_0^2/2$) in Figure 1b, which leads to $\nabla w_x^e = \nabla w_x^m = 0$, and therefore the total gradient vanishes. Second, when the electric fields of the plane waves are parallel (i.e., $\alpha_1=\alpha_2=\pi/2$), the electric and magnetic energy densities exhibit opposite periodic spatial distributions, resulting in mutually antisymmetric gradients ($\nabla w_x^e = -\nabla w_x^m$), and again yielding a vanishing total gradient in Figure 1c. To further investigate the consequences of such field configurations, a Mie dielectric particle (with permittivity $\varepsilon_s = 2.53$, permeability $\mu_s=1$, and radius $R=400$ nm) is placed within the interference field described above, and the longitudinal (along x-axis) optical force acting on the particle is calculated using full-wave simulations. In the case where both w_e and w_m are spatially uniform, no optical force is exerted on the particle, as shown in Figure 1b. This phenomenon can be readily understood, given that the gradient force acting on a dielectric particle primarily arises from the spatial variation in energy density, which is absent when $\nabla w_x = 0$. However, in the antisymmetric configuration where $\nabla w_x^e = -\nabla w_x^m$, a position-dependent longitudinal optical force is found to emerge despite the total energy density gradient being zero in Figure 1c. This counterintuitive result reveals a novel method for modulating the amplitude and sign of the electric and magnetic energy density gradients, as well as interpreting optical forces by exploiting such polarization-tuned antisymmetric mechanisms.

Subsequently, the influence of the polarization state of the incident field on the antisymmetric behavior is investigated at $x=400$ nm. For two plane waves with identical polarization states ($\alpha=\alpha_1=\alpha_2$, $\beta=\beta_1=\beta_2$), Figure 2a and b illustrate the variations in ∇w_x^e and ∇w_x^m as functions of polarization angle α and phase difference β. In this configuration, the gradient distribution simplifies to $\nabla w_x^e = -\nabla w_x^m = -\varepsilon_0 k E_0^2\cos(2\alpha)\sin(2kx)$, indicating that both the magnitude and sign of the energy density

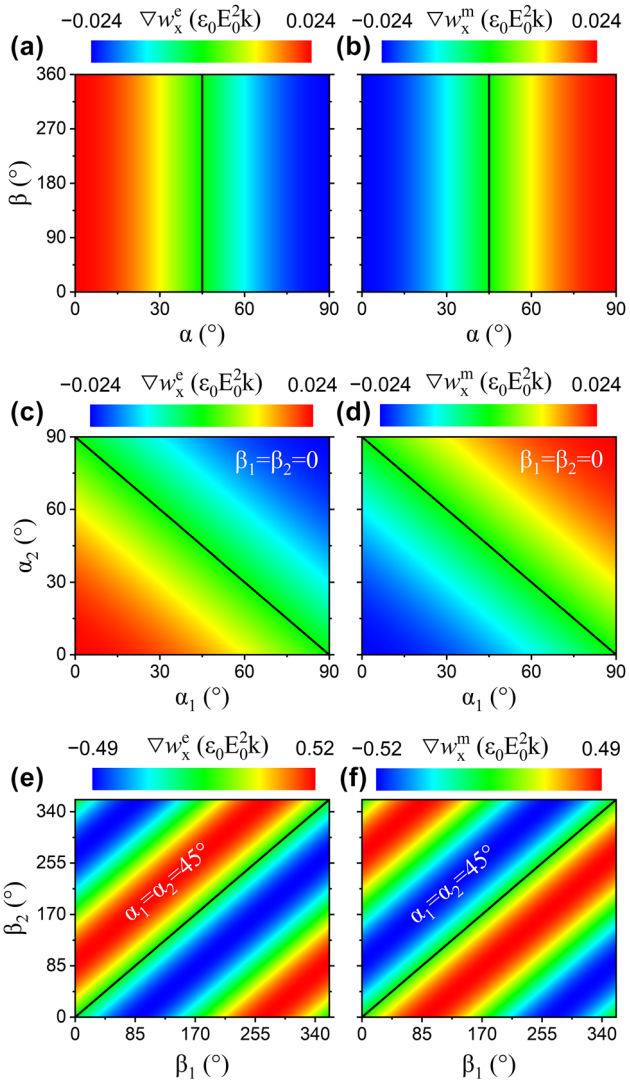

Figure 2: Numerical simulation of polarization-induced antisymmetry in the energy density gradient. The electric (a, c, e) and magnetic (b, d, f) energy density gradients are shown as functions of the polarization angles in two-beam interference fields under various polarization configurations. Black lines indicate conditions under which the electric or magnetic energy density gradient vanishes.

gradients are solely determined by the polarization angle α. The antisymmetric relation holds when $\alpha \neq 45°$, and ∇w_x^e (∇w_x^m) reaches its maximum magnitude at $\alpha = 0°$ or $90°$, corresponding to the strongest longitudinal optical force. In the case where two plane waves are linearly polarized ($\beta_1 = \beta_2 = 0$) with different polarization angles, the gradient takes the form of $\nabla w_x^e = -\nabla w_x^m = -\varepsilon_0 k E_0^2 \cos(\alpha_1 + \alpha_2)\sin(2kx)$. When the polarization angles satisfy $\alpha_1 + \alpha_2 = \pi/2$, interference is suppressed and both ∇w_x^e and ∇w_x^m vanish, as indicated by the black curves in Figure 2c and d. For other polarization configurations, the antisymmetric relationship remains valid. Moreover, a hidden symmetry can be identified, since both ∇w_x^e and ∇w_x^m exhibit antisymmetric distributions with respect to the black curve. For elliptically polarized plane waves with identical polarization angles ($\alpha_1 = \alpha_2 = \pi/4$), the gradient expression becomes $\nabla w_x^e = -\nabla w_x^m = -\varepsilon_0 k E_0^2 [\sin(2kx) - \sin(2kx + \beta_1 - \beta_2)]/2$. It is found that even when both counter-propagating waves are circularly or elliptically polarized with different states ($\beta_1 \neq \beta_2$), the antisymmetric condition is still satisfied. Notably, the amplitude of the electric or magnetic energy density gradient is enhanced by an order of magnitude in the case of non-linearly polarized waves, compared to the linearly polarized scenario. Therefore, the antisymmetry in energy density gradients induced by polarization not only enables a highly efficient mechanism for generating longitudinal optical forces but also offers a flexible approach for modulating their magnitude and direction.

The full-wave simulation method was conducted based on the generalized Lorenz-Mie theory [35] and the Maxwell stress tensor method [36], enabling the determination of the spatial distribution of optical forces acting on spherical particles within the interference field. Apart from the difference in magnitude, both the optical force and the magnetic energy density gradient exhibit identical spatial periodicity, as illustrated in Figure 3a and b, thereby demonstrating a proportional relationship between the optical force and the energy density gradient. To gain an intuitive understanding of the physical mechanism underlying the emergence of longitudinal optical forces, an analytical expression is derived using multipole expansion theory [37] for the optical force acting on an achiral spherical particle under illumination by two counter-propagating plane waves (refer to Supporting Information for more details):

$$\mathbf{F} = \sum_{l=1}^{\infty} \mathbf{F}_{\text{int}}^{(l)} + \sum_{l=1}^{\infty} \mathbf{F}_{\text{rec}}^{(l)}, \tag{4}$$

with

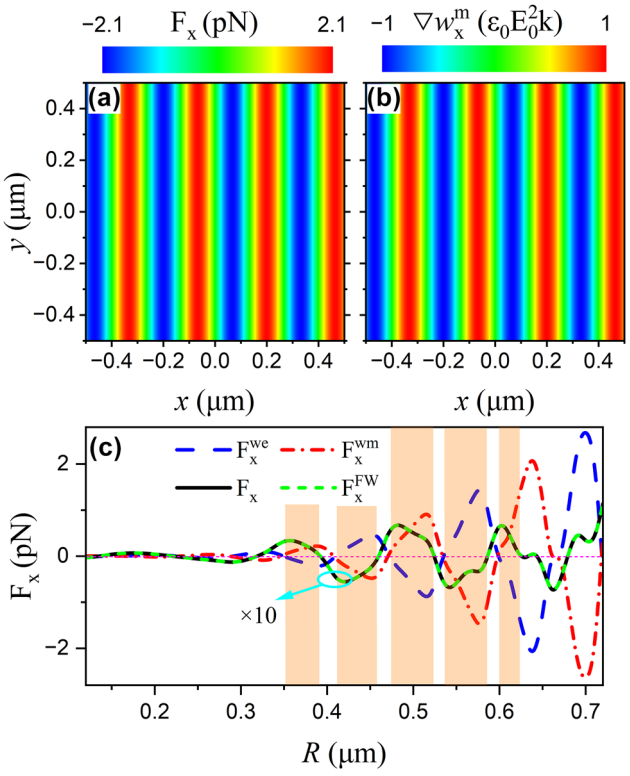

Figure 3: Numerical calculation of the longitudinal optical force on a polystyrene particle immersed in a two-wave interference field. (a) Spatial distribution of the optical force acting on the Mie particle with radius $R = 500$ nm. (b) Corresponding magnetic energy density gradient of the incident light field. (c) Dependence of the longitudinal optical force and its electric and magnetic energy density gradient components on the particle radius. The particle is located at $x = 400$ nm. Full-wave simulation result F_x^{FW} (green dashed lines) is included for comparison. The notation "$\times 10$" indicates that the forces have been magnified by a factor of 10 to enhance visibility. The other parameters are the same as that of Figure 1c.

$$\begin{aligned}
\mathbf{F}_{\text{int}}^{(l)} &= (-1)^l \frac{(2l+1)\pi}{2} \\
&\quad \times \text{Im}\left[(\zeta_l a_l + \xi_l b_l)\nabla w_e + (\xi_l a_l + \zeta_l b_l)\nabla w_m\right], \\
\mathbf{F}_{\text{rec}}^{(l)} &= (-1)^l \chi_l \, \pi \, \text{Im}\left[(\gamma_l a_l^* a_{l+1} + \eta_l b_l^* b_{l+1} + 2\upsilon_l a_l^* b_l)\nabla w_e\right. \\
&\quad \left. + (\eta_l a_l^* a_{l+1} + \gamma_l b_l^* b_{l+1} - 2\upsilon_l a_l^* b_l)\nabla w_m\right],
\end{aligned} \tag{5}$$

and

$$\begin{aligned}
\zeta_l &= l^2 + l + 2, \xi_l = l^2 + l - 2, \\
\gamma_l &= l^2 + 2l + 3, \eta_l = l^2 + 2l - 1, \\
\chi_l &= \frac{l(l+2)}{l+1}, \upsilon_l = \frac{(2l+1)}{l^2(l+2)},
\end{aligned} \tag{6}$$

where l denotes the order of electric and magnetic multipoles, and a_l and b_l represent the Mie coefficients [38]. The interception force $\mathbf{F}_{\text{int}}^{(l)}$ may be interpreted as the response of electromagnetic multipoles to incident fields, whereas the recoil force $\mathbf{F}_{\text{rec}}^{(l)}$ arises from the interplay between various multipoles excited in the particles. To simplify the formula

iteration, we set $E_0 = B_0 = k = \varepsilon_0 = \mu_0 = 1$, to derive the formula in the dimensionless case such that its optical force is in units of $\varepsilon_b E_0^2/k^2$, where ε_b is the dielectric constant of the background. Given that both components are related to the energy density gradient, the total optical force is fundamentally a manifestation of the optical gradient force, viz. $F_x = F_x^g$. Furthermore, the optical force can be decomposed into two contributions, F_x^{we} and F_x^{wm}, corresponding to the gradients of the electric and magnetic energy densities, respectively, i.e. $F_x = F_x^{\mathrm{we}} + F_x^{\mathrm{wm}} = \sum_{l=1}^{\infty} F_x^{\mathrm{we}(l)} + \sum_{l=1}^{\infty} F_x^{\mathrm{wm}(l)}$ where

$$\begin{aligned} F_x^{\mathrm{we}(l)} &= (-1)^l \frac{(2l+1)\pi}{2} \operatorname{Im}[\zeta_l a_l + \xi_l b_l] \nabla w_x^e \\ &\quad + (-1)^l \chi_l \, \pi \operatorname{Im}\left[\gamma_l a_l^* a_{l+1} + \eta_l b_l^* b_{l+1} \right. \\ &\quad \left. + 2\upsilon_l a_l^* b_l\right] \nabla w_x^e, \\ F_x^{\mathrm{wm}(l)} &= (-1)^l \frac{(2l+1)\pi}{2} \operatorname{Im}[\xi_l a_l + \zeta_l b_l] \nabla w_x^m \\ &\quad + (-1)^l \chi_l \, \pi \operatorname{Im}\left[\eta_l a_l^* a_{l+1} + \gamma_l b_l^* b_{l+1} \right. \\ &\quad \left. - 2\upsilon_l a_l^* b_l\right] \nabla w_x^m. \end{aligned} \tag{7}$$

It becomes evident that the gradient force vanishes when both $\nabla w_x^e = 0$ and $\nabla w_x^m = 0$, consistent with the observations in Figure 1b. Figure 3c presents the dependence of the longitudinal gradient force and its components on the particle radius. It can be observed that, for particles within the light orange-shaded region, the contribution from the magnetic energy density gradient surpasses that of its electric counterpart. At specific radii, the total gradient force disappears, which can be attributed to the cancellation of contributions from electric and magnetic multipoles of different orders. However, such cancellation occurs only at discrete radii and thus cannot be interpreted as arising from a universal physical mechanism. Under the specific condition where $\nabla w_x^e = -\nabla w_x^m$, the gradient force ($F_x^g = \sum_{l=1}^{\infty} F_x^{g(l)}$) is further simplified to:

$$\begin{aligned} F_x^{g(l)} = \; & (-1)^l 2(2l+1)\pi \operatorname{Im}[a_l - b_l] \nabla w_x^e \\ & + (-1)^l 4 \chi_l \pi \operatorname{Im}\left[a_l^* a_{l+1} - b_l^* b_{l+1} + \upsilon_l a_l^* b_l\right] \nabla w_x^e. \end{aligned} \tag{8}$$

Most importantly, the gradient force vanishes when the Mie coefficients satisfy the relation:

$$\operatorname{Im}\left[a_l - b_l\right] = 0, \quad \operatorname{Im}\left[a_l^* a_{l+1} - b_l^* b_{l+1} + \upsilon_l a_l^* b_l\right] = 0. \tag{9}$$

This condition is fulfilled when $a_l = b_l$ for all multipolar orders l, indicating that the presence of a particle exhibiting identical electric and magnetic responses results in the disappearance of the gradient force, irrespective of the particle's radius. Hence, the existence of the gradient force is attributed to the breaking of electromagnetic symmetry induced by the particle. Moreover, Eqs. (5) and (8) reveal that, in addition to electromagnetic symmetry breaking, the emergence of longitudinal gradient forces necessitates a gradient in the electric or magnetic energy density, which is shown in Eq. (3) to depend on the polarization angle and the phase difference. Consequently, even when the irradiance acting on an isotropic particle does not produce a net energy density gradient along the x-direction, an underlying antisymmetry in the gradient field persists. This antisymmetry facilitates the coupling between particles with electromagnetic symmetry breaking and light, thereby generating anomalous longitudinal gradient forces. Additionally, as demonstrated in Figure 2, the polarization angle in Eq. (3) determines the direction of the longitudinal gradient force, which can be reversed by altering this angle. Of particular interest in this case is the observation that the magnitude of the gradient force can reach its maximum under elliptically polarized illumination, rather than with circular or linearly polarized light (refer to Figures S2 and S3 in the Supporting Information). Additionally, according to Eq (3) it is evident that the electric and magnetic energy density gradients are position dependent. The numerical results demonstrate that, within a certain spatial region, the maximum values of the electric or magnetic energy density gradient at different positions correspond to different polarization state configurations. As a result, the longitudinal gradient force can be significantly enhanced by a larger energy density gradient. This provides a controllable mechanism for tailoring the amplitude and directionality of the longitudinal force via polarization modulation.

To gain deeper insight into the physical origin of gradient forces induced by electromagnetic symmetry breaking, Figure 4a shows that the gradient force is plotted as a function of the particle's relative permittivity ε_s and permeability μ_s, for a particle of 400 nm radius located at $x = 400$ nm. The black solid line indicates the condition $\varepsilon_s/\varepsilon_b = \mu_s/\mu_b$, corresponding to identical electric and magnetic responses, where ε_b and μ_b are the background permittivity and permeability, respectively. As illustrated in Figure 4a, when the particle is immersed in vacuum, a gradient force emerges if $\varepsilon_s \neq \mu_s$, indicating that electromagnetic symmetry has been broken. The gradient force also exhibits antisymmetry with respect to the solid black line, i.e., $F_x^g(\varepsilon_s/\varepsilon_b, \mu_s/\mu_b) = -F_x^g(\mu_s/\mu_b, \varepsilon_s/\varepsilon_b)$, regardless of the particle size. Thus, for an isotropic and achiral particle of arbitrary size and composition, the condition $\varepsilon_s/\varepsilon_b \neq \mu_s/\mu_b$ leads to the emergence of a gradient force in an optical field that possesses antisymmetry in the electric and magnetic energy density

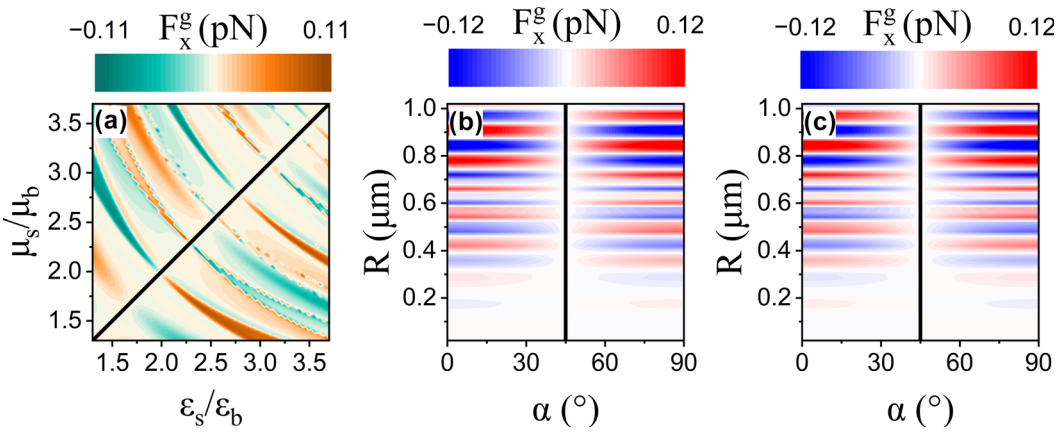

Figure 4: The longitudinal optical gradient force arising from the electromagnetic symmetry breaking of the particle. (a) Dependence of the gradient force on the particle's relative permittivity $\varepsilon_s/\varepsilon_b$ and relative permeability μ_s/μ_b, with the particle immersed in vacuum. (b–d) Gradient force as a function of the polarization angle α and the particle radius R for two representative sets of electromagnetic parameters: (ε_s, μ_s) = (2.53, 1.0) in (b), (1.0, 2.53) in (c). The black solid lines indicate the conditions under which the optical gradient force disappears. All other parameters are the same as that of Figure 3c.

gradients. When this antisymmetry between two components is broken, a gradient force can be generated even on particles with electromagnetic symmetry, as described in Figure S4 from the Supporting Information.

Furthermore, for particles with different ε_s and μ_s, the dependence of the gradient force on both the polarization angle α and the particle radius R (ranging from the Rayleigh to the Mie scattering regime) is evaluated and presented in Figure 4b and c, respectively. No gradient force is observed across the entire parameter space for the symmetric case $\varepsilon_s = \mu_s = 2.53$. The black curves denote the polarization angles at which the gradient force vanishes, corresponding to the absence of both electric and magnetic energy density gradients at $\alpha = 45°$ (consistent with Figure 2a and b). Intuitively, with a fixed polarization angle, variations in particle radius modulate both the magnitude and direction of the gradient force (consistent with Figure 3c). Moreover, for a fixed particle radius, the gradient force can be tuned by varying α, following a cosine $\cos(2\alpha)$ dependence, independent of the particle's size and composition. Notably, the gradient force reaches its maximum when $\alpha = 0°$ or 90°, implying that the maximum electric (or magnetic) energy density gradient is achieved at these angles. Similar trends are observed in Figure 4c for the case (ε_s, μ_s)=(1, 2.53). A comparison between Figure 4b and c confirms the antisymmetric property $F_x^g(2.53, 1) = -F_x^g(1, 2.53)$. In contrast, the absence of a longitudinal gradient force for $\varepsilon_s = \mu_s = 2.53$ can be attributed to the presence of electromagnetic symmetry. These results highlight the significant influence of both the polarization angle and particle radius on the magnitude and direction of the longitudinal gradient force. The ability to tune this force by adjusting the polarization angle provides new insights for optimizing optical manipulation.

3 Conclusions

While optical gradient forces have traditionally been regarded as a consequence of spatial variations in the intensity of the optical field, recent investigations have revealed that similar forces may also arise from gradients in more complex optical field quantities, such as the helicity density gradient [20]–[24] or the magneto-electric energy density gradient [25], albeit predominantly in systems involving chiral particles. In contrast to these earlier findings, the present work has demonstrated the existence of an unconventional gradient force that acts on isotropic, achiral spherical particles immersed in an interference field generated by two counter-propagating plane waves, wherein the total energy density gradient vanishes as a result of a polarization-tuned antisymmetry between its electric and magnetic components in the interference field. By establishing a general analytical expression for the gradient force exerted on particles of arbitrary size, it has been explicitly shown that the underlying physical origin of the observed force can be attributed to the particle-induced breaking of electromagnetic symmetry, which, in turn, couples to the antisymmetric structure of the energy density gradients inherent to the interfering field. Moreover, it has been found that the antisymmetry of the electric and magnetic energy density gradient distributions, can be effectively disrupted through appropriate adjustment of the illumination parameters, particularly the incident angle and polarization

orientation, thereby enabling the generation of an optical gradient force even in the electric-magnetic symmetry of the particle. Of particular interest is the observation that the magnitude of the electric-magnetic symmetry-breaking-induced gradient force may reach its maximum value not under circular or linearly polarized light, but rather under elliptically polarized illumination at the specific position. Furthermore, through a systematic variation of the particle radius across the Rayleigh and Mie scattering regimes, it has been revealed that the contribution of the magnetic energy density gradient to the total optical force may, under certain conditions, surpass that arising from the electric component, thereby highlighting the critical role played by the magnetic energy density gradient in determining the overall force profile. These results not only deepen the fundamental understanding of light–matter interactions in structured fields but also offer novel opportunities for tailoring optical forces through the precise engineering of polarization states and material responses.

Supporting Information

Numerical simulations of the energy density gradient under illumination by two plane waves with different incident angles are performed; the analytical derivation of optical forces on multipoles in two-wave interference is presented; the influence of the polarization state of the incident field on the optical gradient force is investigated; the breaking of antisymmetry in the electric and magnetic energy density gradients is analyzed.

Research funding: National Natural Science Foundation of China (12274074, 12134013). Natural Science Foundation of Jiangsu Province (BK20242024). Postgraduate Research & Practice Innovation Program of Jiangsu Province (KYCX24_0381).

Author contribution: LF and ZS contributed equally to the paper. LF and ZS performed the numerical simulations. RZ, ZL, and BL helped with the theoretical analysis. All authors were involved in the discussion and analysis. GR coordinated all the work. All authors have accepted responsibility for the entire content of this manuscript and consented to its submission to the journal, reviewed all the results and approved the final version of the manuscript.

Conflict of interest: Authors state no conflict of interest.

Data availability: The datasets generated and/or analysed during the current study are available from the corresponding author upon reasonable request.

References

[1] J. Baumgartl, M. Mazilu, and K. Dholakia, "Optically mediated particle clearing using Airy wavepackets," *Nat. Photonics*, vol. 2, no. 11, pp. 675–678, 2008.

[2] J. Chen, J. Ng, Z. Lin, and C. T. Chan, "Optical pulling force," *Nat. Photonics*, vol. 5, no. 9, pp. 531–534, 2011.

[3] S. Sukhov and A. Dogariu, "Negative nonconservative forces: optical 'tractor beams' for arbitrary objects," *Phys. Rev. Lett.*, vol. 107, no. 20, p. 203602, 2011.

[4] D. G. Grier, "A revolution in optical manipulation," *Nature*, vol. 424, no. 6950, pp. 810–816, 2003.

[5] M. L. Juan, M. Righini, and R. Quidant, "Plasmon nano-optical tweezers," *Nat. Photonics*, vol. 5, no. 6, pp. 349–356, 2011.

[6] M. Padgett and R. Bowman, "Tweezers with a twist," *Nat. Photonics*, vol. 5, no. 6, pp. 343–348, 2011.

[7] R. W. Bowman and M. J. Padgett, "Optical trapping and binding," *Rep. Prog. Phys.*, vol. 76, no. 2, p. 026401, 2013.

[8] J. Kepler, *De Cometis Libelli Tres*, Augsburg, Augustae Vindelicorum, 1619.

[9] A. Ashkin, "Acceleration and trapping of particles by radiation pressure," *Phys. Rev. Lett.*, vol. 24, no. 4, p. 156, 1970.

[10] A. Ashkin, J. M. Dziedzic, J. E. Bjorkholm, and S. Chu, "Observation of a single-beam gradient force optical trap for dielectric particles," *Opt. Lett.*, vol. 11, no. 5, pp. 288–290, 1986.

[11] V. Ginis, P. Tassin, C. M. Soukoulis, and I. Veretennicoff, "Enhancing optical gradient forces with metamaterials," *Phys. Rev. Lett.*, vol. 110, no. 5, p. 057401, 2013.

[12] M. Woerdemann, C. Alpmann, M. Esseling, and C. Denz, "Advanced optical trapping by complex beam shaping," *Laser Photonics Rev.*, vol. 7, no. 6, pp. 839–854, 2013.

[13] M. E. J. Friese, T. A. Nieminen, N. R. Heckenberg, and H. Rubinsztein-Dunlop, "Optical alignment and spinning of laser-trapped microscopic particles," *Nature*, vol. 394, no. 6691, pp. 348–350, 1998.

[14] O. M. Maragò, P. H. Jones, P. G. Gucciardi, G. Volpe, and A. C. Ferrari, "Optical trapping and manipulation of nanostructures," *Nat. Nanotech.*, vol. 8, no. 11, pp. 807–819, 2013.

[15] M. Daly, M. Sergides, and S. Nic Chormaic, "Optical trapping and manipulation of micrometer and submicrometer particles," *Laser Photonics Rev.*, vol. 9, no. 3, pp. 309–329, 2015.

[16] Y. Yang, Y. X. Ren, M. Chen, Y. Arita, and C. Rosales-Guzmán, "Optical trapping with structured light: a review," *Adv. Photonics*, vol. 3, no. 3, p. 034001, 2021.

[17] M. C. Zhong, X. B. Wei, J. H. Zhou, Z. Q. Wang, and Y. M. Li, "Trapping red blood cells in living animals using optical tweezers," *Nat. Commun.*, vol. 4, p. 1768, 2013.

[18] G. Tkachenko and E. Brasselet, "Helicity-dependent three-dimensional optical trapping of chiral microparticles," *Nat. Commun.*, vol. 5, p. 4491, 2014.

[19] W. Lu, A. V. Krasavin, S. Lan, A. V. Zayats, and Q. Dai, "Gradient-induced long-range optical pulling force based on photonic band gap," *Light Sci. Appl.*, vol. 13, p. 93, 2024.

[20] Y. Zhao, A. A. E. Saleh, and J. A. Dionne, "Enantioselective optical trapping of chiral nanoparticles with plasmonic tweezers," *ACS Photonics*, vol. 3, no. 3, pp. 304–309, 2016.

[21] L. Fang and J. Wang, “Optical trapping separation of chiral nanoparticles by subwavelength slot waveguides,” *Phys. Rev. Lett.*, vol. 127, no. 23, p. 233902, 2021.
[22] J. Yamanishi, *et al*., “Optical gradient force on chiral particles,” *Sci. Adv.*, vol. 8, no. 38, p. eabq2604, 2022.
[23] Y. Zhang, *et al*., “Enantioselective optical trapping of multiple pairs of enantiomers by focused hybrid polarized beams,” *Small*, vol. 20, no. 25, p. 2309395, 2024.
[24] R. Jin, *et al*., “Harnessing enantioselective optical forces by quasibound states in the continuum,” *Phys. Rev. Lett.*, vol. 133, no. 8, p. 086901, 2024.
[25] H. Zheng, H. Chen, J. Ng, and Z. Lin, “Optical gradient force in the absence of light intensity gradient,” *Phys. Rev. B*, vol. 103, no. 3, p. 035103, 2021.
[26] J. A. Rodrigo, M. Angulo, and T. Alieva, “All-optical motion control of metal nanoparticles powered by propulsion forces tailored in 3D trajectories,” *Photonics Res.*, vol. 9, no. 1, pp. 1—12, 2020.
[27] Y. Roichman, B. Sun, Y. Roichman, J. Amato-Grill, and D. G. Grier, “Optical forces arising from phase gradients,” *Phys. Rev. Lett.*, vol. 100, no. 1, p. 013602, 2008.
[28] J. A. Rodrigo, T. Alieva, V. Manzaneda-González, and A. Guerrero-Martínez, “All-optical trapping and programmable transport of gold nanorods with simultaneous orientation and spinning control,” *ACS Nano*, vol. 18, no. 40, pp. 27738—27751, 2024.
[29] K. Y. Bliokh, A. Y. Bekshaev, and F. Nori, “Dual electromagnetism: helicity, spin, momentum and angular momentum,” *New J. Phys.*, vol. 15, no. 3, p. 033026, 2013.
[30] M. V. Berry, “Optical currents,” *J. Opt. A*, vol. 11, no. 9, p. 094001, 2009.
[31] C. J. Min, *et al*., “Focused plasmonic trapping of metallic particles,” *Nat. Commun.*, vol. 4, 2013, Art. no. 2891.
[32] R. P. Cameron, S. M. Barnett, and A. M. Yao, “Discriminatory optical force for chiral molecules,” *New J. Phys.*, vol. 16, no. 1, p. 013020, 2014.
[33] S. Sukhov and A. Dogariu, “Non-conservative optical forces,” *Rep. Prog. Phys.*, vol. 80, no. 11, p. 112001, 2017.
[34] X. Yu, *et al*., “Anomalous lateral optical force as a manifestation of the optical transverse spin,” *Laser Photonics Rev.*, vol. 17, no. 10, p. 2300212, 2023.
[35] G. Gouesbet and G. Grehan, *Generalized Lorenz-Mie Theories*, Berlin, Springer, 2011.
[36] Q. Ye and H. Lin, “On deriving the Maxwell stress tensor method for calculating the optical force and torque on an object in harmonic electromagnetic fields,” *Eur. J. Phys.*, vol. 38, no. 4, p. 045202, 2017.
[37] H. Zheng, X. Li, Y. Jiang, J. Ng, Z. Lin, and H. Chen, “General formulations for computing the optical gradient and scattering forces on a spherical chiral particle immersed in generic monochromatic optical fields,” *Phys. Rev. A*, vol. 101, no. 5, p. 053830, 2020.
[38] C. F. Bohren and D. R. Huffman, *Absorption and Scattering of Light by Small Particles*, New York, John Wiley, 1998.

Supplementary Material: This article contains supplementary material (https://doi.org/10.1515/nanoph-2025-0223).